Neuron
Article

Nitric Oxide Is a Volume Transmitter Regulating Postsynaptic Excitability at a Glutamatergic Synapse

Joern R. Steinert,[1] Cornelia Kopp-Scheinpflug,[2] Claire Baker,[1] R.A. John Challiss,[3] Raj Mistry,[3] Martin D. Haustein,[1] Sarah J. Griffin,[1] Huaxia Tong,[1] Bruce P. Graham,[4] and Ian D. Forsythe[1,*]
[1]MRC Toxicology Unit, Hodgkin Building, University of Leicester, Leicester LE1 9HN, UK
[2]Institute of Biology II, Faculty of Biosciences, Pharmacy and Psychology, University of Leipzig, Talstraße 33, 04103 Leipzig, Germany
[3]Department of Cell Physiology and Pharmacology, University of Leicester, Leicester LE1 9HN, UK
[4]Department of Computing Science and Mathematics, University of Stirling, Stirling FK9 4LA, UK
*Correspondence: idf@le.ac.uk
DOI 10.1016/j.neuron.2008.08.025

SUMMARY

Neuronal nitric oxide synthase (nNOS) is broadly expressed in the brain and associated with synaptic plasticity through NMDAR-mediated calcium influx. However, its physiological activation and the mechanisms by which nitric oxide (NO) influences synaptic transmission have proved elusive. Here, we exploit the unique input-specificity of the calyx of Held to characterize NO modulation at this glutamatergic synapse in the auditory pathway. NO is generated in an activity-dependent manner by MNTB principal neurons receiving a calyceal synaptic input. It acts in the target neuron and adjacent inactive neurons to modulate excitability and synaptic efficacy, inhibiting postsynaptic Kv3 potassium currents (via phosphorylation), reducing EPSCs and so increasing action potential duration and reducing transmission fidelity. We conclude that NO serves as a volume transmitter and slow dynamic modulator, integrating spontaneous and evoked neuronal firing, thereby providing an index of global activity and regulating information transmission across a population of active and inactive neurons.

INTRODUCTION

Nitric oxide is a crucial signaling molecule in cardiovascular (Ignarro et al., 1987; Palmer et al., 1987), reproductive (Hurt et al., 2006), immune (Bogdan, 2001), and central nervous systems (Garthwaite, 2008; Bon and Garthwaite, 2003; Bredt et al., 1990). NO exhibits properties ideally suited for a transcellular messenger: being highly soluble and mobile (unimpeded by cell membranes), widely synthesized and of limited lifetime. It acts via a well-characterized NO-cGMP pathway (Southam and Garthwaite, 1993), although S-nitrosylation of proteins, generation of reactive oxygen species, and regulation of cellular respiration also contribute to physiological and pathological roles (Ahern et al., 2002). In the brain, nNOS is expressed widely in the neocortex, cerebellum, and hippocampus and is closely associated with NMDAR (Brenman et al., 1996) and synaptic plasticity (Hopper and Garthwaite, 2006; Jacoby et al., 2001; Son et al., 1996). NO has the potential to act as an anterograde or retrograde modulator, but its mechanisms of controlling neuronal excitability in the brain are not well characterized.

We have exploited a glutamatergic synapse in the auditory brainstem, called the calyx of Held (Forsythe, 1994; Schneggenburger and Forsythe, 2006; von Gersdorff and Borst, 2002), to study the cellular mechanism of NO signaling. This giant synapse forms on principal neurons in the medial nucleus of the trapezoid body (MNTB). Each neuron receives one calyx, which generates a stereotypical dual-component response: a fast AMPAR-mediated and slow NMDAR-mediated EPSC (Barnes-Davies and Forsythe, 1995; Forsythe and Westbrook, 1988; Futai et al., 2001; Joshi and Wang, 2002). The morphology of the calyx is analogous to an axon terminal field enveloping a single neuronal soma, so providing the ultimate input-specificity of one synapse to one target neuron. This giant synapse serves as a relay in pathways responsible for sound localization, by comparison of auditory information from both cochleae (Oertel, 1999). The MNTB expresses high levels of several crucial elements in NO signaling, including nNOS and soluble guanylyl cyclase (sGC) (Fessenden et al., 1999; Lein et al., 2007).

Concepts of plasticity often focus on changes in synaptic strength, but the synaptic response must also integrate with the intrinsic voltage-gated currents of the target neuron to generate an action potential (AP) output. Therefore, modulation of these postsynaptic intrinsic conductances contributes to neuronal excitability (Daoudal and Debanne, 2003; Marder and Prinz, 2002) and also synaptic efficacy. For example, in the MNTB, AP firing threshold and excitability are regulated by Kv1 channels (Brew and Forsythe, 2005; Dodson et al., 2002), while AP duration and firing rates are influenced by Kv3 channels (Wang et al., 1998). Kv3 channels are widely expressed in fast-spiking neurons (Rudy and McBain, 2001), and, in the auditory system, their activity is regulated by sound-evoked changes in phosphorylation (Song et al., 2005). In this paper, we identify a form of activity-dependent signaling mediated by NO, which acts over relatively slow timescales (5–30 min), consistent with a physiological role in tuning a neuronal population to the volume-average of local spontaneous and evoked synaptic activity.

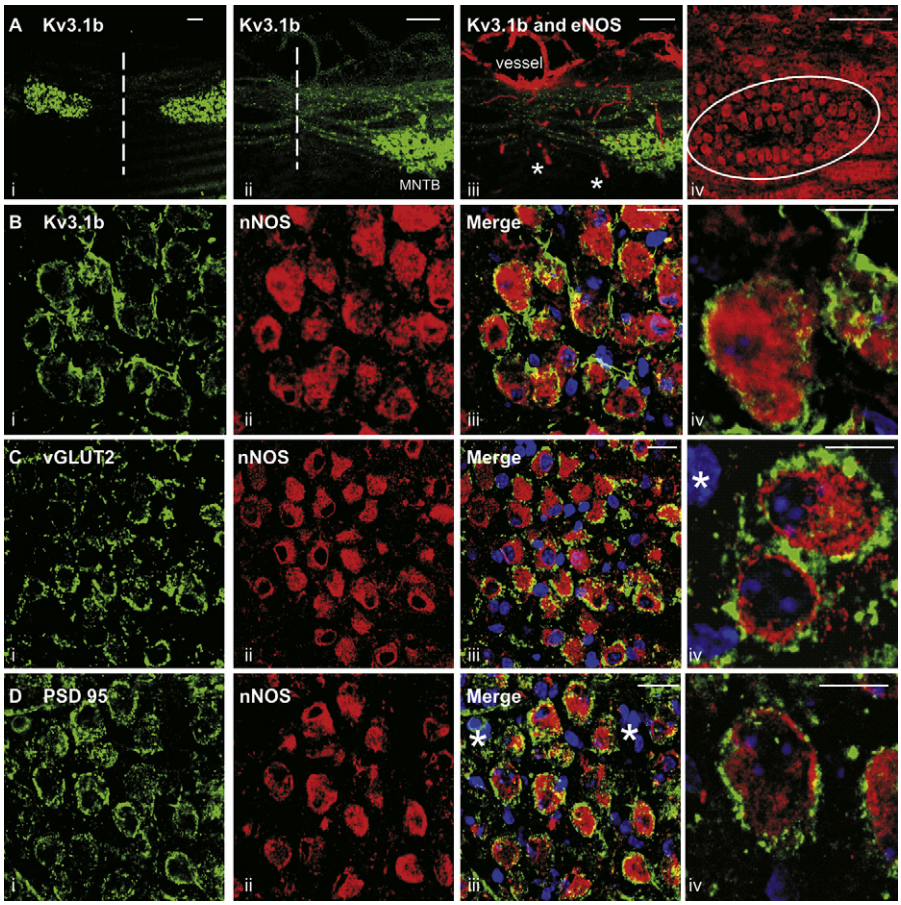

Figure 1. nNOS Is Expressed in Postsynaptic MNTB Neurons

(Ai and Aii) Each panel shows low-magnification images of the superior olivary complex at the midline (dashed line) in a transverse section, with bilateral MNTB nuclei stained by an antibody against Kv3.1b (NeuroMab). (Aiii) Colabeling of the (Aii) section with an eNOS antibody (BD Transduction Lab.) shows high expression in the ventral blood vessel and capillaries (*) but no neuronal localization. (Aiv) In contrast, a nNOS antibody (SantaCruz) shows high expression across the MNTB (circled).

(Bi–Div) Each panel is a confocal fluorescence image of MNTB neurons stained with the nNOS antibody (red) colocalized with: (B) the K^+ channel subunit Kv3.1b (green); (C) the presynaptic marker vGLUT2 (green, Chemicon), and (D) PSD95 (green, AbCam). (Biii–Diii) Merged images include DAPI-stained nuclei, and the far right images (Biv–Div) show single optical sections from each projected confocal image.

Scale bars: (Ai–Aiv) 100 μm, (Bi–Diii) 20 μm, (Biv–Div) 10 μm.

RESULTS

nNOS Is Expressed at Postsynaptic Sites in MNTB Neurons

MNTB neurons and the calyx of Held express the voltage-gated K^+ channel Kv3.1b (Elezgarai et al., 2003; Wang et al., 1998), and antibodies to this channel clearly show the bilateral location of the MNTB in transverse cryostat sections of the superior olivary complex (SOC, Figure 1A) in the auditory brainstem. In this region, endothelial NOS (eNOS) was localized to blood vessels on the ventral surface and within capillaries but was not detectable in MNTB neurons or glial cells, as emphasized by the separate localization of eNOS and Kv3.1b. In contrast, an antibody to nNOS showed strong labeling of the MNTB (Figure 1Aiv). Colabeling of Kv3.1b with the vesicular glutamate transporter-2 (vGLUT2) (Billups, 2005) and with nNOS showed that Kv3.1b (green, Figure 1B) was largely present in membranes, while nNOS (red) was located in the cytoplasm of MNTB principal neurons. The localization of either vGLUT2 (green, Figure 1C) or PSD-95 (green, Figure 1D) with Kv3.1b clearly shows the synaptic profiles of the calyx around each neuron, emphasizing the postsynaptic cytoplasmic location of nNOS (red). DAPI staining showed principal neurons with prominent nucleoli (Figures 1C and 1D, *).

Nitric Oxide Is Generated on Synaptic Stimulation

To investigate the role of NO in auditory brainstem signaling, we used the fluorescent probe DAR-4M (Kojima et al., 2001) to monitor NO production in brainstem slice preparations of the mouse SOC. Presynaptic calyceal APs were evoked using midline bipolar stimulation at 36°C–37°C (Billups et al., 2002) and stimulation rates of up to 100 Hz. These rates of synaptic stimulation were well within the auditory pathway physiological range for both spontaneous and sound-driven inputs. High levels of

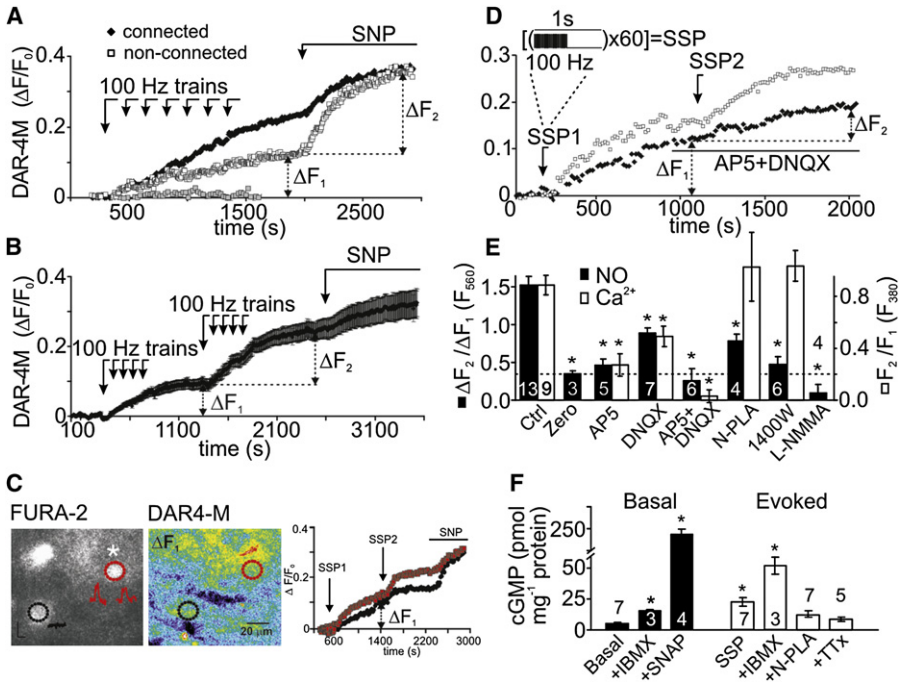

Figure 2. NO and cGMP Are Generated on Stimulation of the Calyx of Held

(A) Stimulation of the calyceal presynaptic axons in the trapezoid body (100 Hz trains for 120 s repeated seven times) increased DAR-4M fluorescence, indicating NO accumulation in neurons possessing a functional calyx (filled squares); less accumulation was observed in neighboring nonconnected neurons (open squares); both connected and nonconnected neurons increased fluorescence in response to the NO donor, SNP (800 μM). Neurons in control slices receiving no stimulation (open symbols, bottom trace) showed no change in fluorescence.

(B) Repetition of the two stimulus trains (arrow, SSP = [100 Hz trains for 500 ms repeated at 1 Hz for 60 s] × 5) showed that each train generated increased NO in connected neurons (n = 3), and SNP application further increased the response.

(C) Fura-2 image of three MNTB neurons (380 nm ex., left) and DAR-4M fluorescence (560 nm ex., middle). Two consecutive SSP trains show raised $[Ca^{2+}]_i$ (red circle and trace, 340/380 nm ratio) in the connected neuron but no change in the nonconnected MNTB neuron (black circle and trace, 340/380 nm ratio). The time course of DAR-4M fluorescence changes ($\Delta F/F_o$) for both cells is plotted (right) for the connected (red) and nonconnected (black) neuron showing increased NO with each SSP and for SNP.

(D) Time course of DAR-4M fluorescence change following two stimulus trains (SSP1 and SSP2) in the absence (open symbols) or presence (closed symbols) of DNQX (10 μM) and AP5 (50 μM) during SSP2.

(E) Summary of the pharmacology for fluorescent detection of NO (filled bars, left axis) and $\Delta[Ca^{2+}]_i$ (open bars, right axis). Bar labeled "Zero" and dotted line indicate the zero response to SSP2. AP5 (50 μM) and DNQX (10 μM) reduced NO and $[Ca^{2+}]_i$ accumulation following SSP2. Competitive NOS antagonists L-NMMA (500 μM), N-PLA (10 μM), and 1400W (10 μM) blocked NO accumulation but not $[Ca^{2+}]_i$ (Ca^{2+} was not measured for L-NMMA); ANOVA, *$p < 0.05$.

(F) cGMP production in response to synaptic stimulation of the trapezoid body: basal cGMP was increased by phosphodiesterase inhibition (IBMX, 500 μM) and massively increased by the NO donor SNAP (100 μM). Calyceal stimulation (SSP) also increased cGMP, with further potentiation by IBMX. Synaptic cGMP accumulation was blocked by N-PLA (10 μM) and by blocking AP propagation with tetrodotoxin (1 μM). Students t test, *$p < 0.05$. All data are means ± SEM, n is indicated by the respective numeral in each case.

spontaneous firing are a feature of the auditory pathway (Liberman and Oliver, 1984), with the mouse MNTB having spontaneous rates between 0 and 150 Hz, and peak sound-evoked firing rates can exceed 700 Hz in vivo (Kopp-Scheinpflug et al., 2008). The slice preparation divides MNTB neurons into two groups: those with an intact calyceal input (connected) and the majority, without an intact calyx (nonconnected), caused by severing the axon when cutting the brain slice. Spontaneous AP firing of MNTB neurons in an in vitro slice is rare (<<1 Hz) since there is no intact input from the cochlea.

Following a 5 min control period (Figure 2A), calyceal axons were stimulated (indicated by each arrow) at 100 Hz, seven times (each 120 s), and DAR-4M fluorescence changes were monitored. A connected MNTB neuron possessing an intact calyceal input ("connected") showed a slow increase in DAR-4M fluorescence (Figure 2A, filled symbols, data expressed as $\Delta F/F_0$ [$t_{1/2}$ = 679 ± 42 s, n = 14]). The nonconnected cell showed a smaller magnitude change (open symbols), but no change in fluorescence was observed in another preparation in the absence of stimulation (gray symbols). The DAR-4M/NO reaction is irreversible, so termination of NO production is observed as a declining rate of increase following stimulation; the asymptote is not dye depletion, since application of the NO-donor sodium nitroprusside (SNP) increased fluorescence of both connected and nonconnected neurons to a similar level. In averaged data from three connected neurons (Figure 2B), delivery of two identical 100 Hz trains led to a biphasic rise of DAR-4M fluorescence that also increased further with SNP.

To aid quantification and pharmacological characterization of NO production, we used two identical consecutive stimulus trains

(Figure 2C). Each is referred to as a "synaptic stimulus protocol" (SSP), consisting of a 60 s, 100 Hz train with a 50% duty cycle (SSP = 60 s at 100 Hz, 500 ms on, 500 ms off; i.e., an average of 50 Hz over 1 min). The two SSPs were separated by 1000 s, and each caused increases in $[Ca^{2+}]_i$ in connected MNTB neurons and a reproducible DAR-4M fluorescence change (in paired experiments on the same slice). A single Fura-2 image at 380 nm shows (Figure 2C, left) a connected (red circle) and a nonconnected (black circle) MNTB neuron with the 340/380 nm fluorescence ratio plotted during synaptic stimulation (red and black insets, respectively). The change in DAR-4M fluorescence (ΔF_1) is shown in the middle image and plotted over time in Figure 2C, right ($\Delta F/F_0$). The actions of pharmacological agents were assessed as the ratio of signal differences ($\Delta F_2/\Delta F_1$) between the first control SSP ($\Delta F_1 = \Delta F_{1100s}$-$\Delta F_{100\,s}$) and the second test SSP ($\Delta F_2 = \Delta F_{2000s} - \Delta F_{1000s}$). Figure 2D shows a single cell receiving two SSP stimuli (open symbols) overlaid with data from another slice showing suppression of the SSP2 response by glutamate receptor antagonists (Figure 2D, filled symbols). Because of the continued increase in DAR-4M fluorescence following SSP1, the measured SSP2 fluorescence signal was larger than that for SSP1. The continued accumulation from SSP1 was measured at both ΔF_1 and ΔF_2 time points (Figure 2E, 1xSSP = zero, $\Delta F_2/\Delta F_1 = 0.35 \pm 0.28$, n = 3). Because of this small continued increase, the dashed line in the summary data (Figure 2E) gives the best estimate for a zero response to SSP2. Under control conditions, $\Delta F_2/\Delta F_1$ is larger than 1 ($\Delta F_2/\Delta F_1 = 1.51 \pm 0.12$, n = 13), suggesting potentiation of NO production for the second stimulus. Perfusion of glutamate receptor antagonists following SSP1, resulted in reduced $\Delta F_2/\Delta F_1$ ratios for NO production (Figure 2E, filled bars) and reduced $[Ca^{2+}]_i$ for SSP2 (open bars). The NMDAR antagonist AP-5 blocked NO accumulation at all animal ages tested (up to P21, Figure S4B). The AMPAR antagonist DNQX also partially blocks NMDAR, and so reduced NO accumulation when applied alone, but the absence of NO accumulation in AP-5 implies that Ca^{2+}-permeable AMPAR expressed in the MNTB (Joshi et al., 2004) make little or no contribution to nNOS activation. Competitive NOS antagonists, N-PLA (10 μM), L-NMMA (500 μM), and 1400W (10 μM), each suppressed DAR-4M fluorescence ratios $\Delta F_2/\Delta F_1$ but left SSP2-evoked $[Ca^{2+}]_i$ increases unaffected (Figure 2E, open bars for N-PLA and L-NMMA). These results are consistent with NMDAR- and calcium-dependent induction of nNOS and suggest little involvement of endothelial or inducible NOS isoforms (Hopper and Garthwaite, 2006).

Synaptic Activity Induces cGMP Accumulation

A key action of NO is activation of sGC and generation of intracellular cGMP. Measurement of cGMP was performed (using the same in vitro slice preparation) in response to perfusion of NO-donors and after presynaptic stimulation (SSP). Low basal cGMP concentrations were enhanced by inhibition of phosphodiesterases (IBMX, 0.5 mM) in control nonstimulated slices (Figure 2F) and were unchanged by perfusion with Bay 41-2272, an allosteric enhancer of the sGC activity (1 μM, data not shown), suggesting little basal sGC activity at rest in vitro. Perfusion of the NO donor SNAP (100 μM) increased cGMP concentrations by two orders of magnitude. Electrical stimulation of the presynaptic axons in the MNTB showed that a physiological stimulus also raised cGMP, and this was further potentiated by IBMX. Despite the small number of intact calyceal axons, we still detected strong cGMP production, and this increase was blocked by tetrodotoxin or by inhibition of nNOS with N-PLA (10 μM), confirming generation of cGMP on synaptic stimulation through an nNOS-dependent mechanism.

Nonsynaptic Volume Transmission by NO

NO has long been considered a putative volume transmitter, but it is difficult to prove this concept in most brain areas, where synaptic inputs are distributed between many neurons. Visualization of transneuronal NO diffusion in the MNTB was achieved using DAR-4M and calcium imaging. Figure 3A shows two neurons in which one receives a calyceal input (*, red circle). On delivery of two SSPs, this neuron exhibited sustained large changes in $[Ca^{2+}]_i$ (red trace, inset) while a noninnervated neuron (black circle) showed no change in $[Ca^{2+}]_i$ (black trace, inset). Following SSP1, the ΔF_1 image shows a global increase in fluorescence (Figure 3A, ΔF_1), and a plot of the DAR-4M $\Delta F/F_0$ against time (Figure 3A, right) shows clear NO accumulation after SSP1 in both neurons (red, connected; black, nonconnected). Perfusion of the NO scavenger, PTIO (Figure 3A, ΔF_2) prior to the second SSP suppressed the fluorescent *increase* in the noninnervated neuron and surrounding tissue (Figure 3A, right, black symbols after SSP2), although the innervated neuron continued to respond (Figure 3A, right, red symbols after SSP2). A line scan for this same data is shown in Figure 3B (data plot along the 100 μm white line in Figure 3A). The innervated neuron (*) shows high fluorescence following SSP1, while the nonconnected neuron (#) also shows substantial fluorescence (ΔF_1, black trace). Following perfusion by PTIO (ΔF_2, gray trace), the increase in background fluorescence is suppressed everywhere, while the innervated neuron still shows a rise in NO fluorescence. Averaging the fluorescence intensities for ΔF_1 and ΔF_2 measured over four innervated neurons ("On Cell") versus the 20 μm either side of the same neuron ("Off Cell") in the absence (filled bars) and presence of PTIO during the second SSP (gray bars) shows that NO diffusion was prevented by scavenging (Figure 3C).

Further evidence for the diffusion of NO was obtained by estimating NO accumulation with distance from known sources. The NO concentration gradient was estimated from the rate of change of DAR-4M fluorescence and plotted against distance from a single neuron source following one SSP. The rate of change decreased proportionally to the distance from the source neuron (Figure 3D) compared with the response to perfusing an NO donor, where the gradient did not change with distance. Numerical simulation of NO spread was made within a block of neural tissue (Figure S1). A 20 μm diameter spherical constant-rate source of NO gives a highly localized [NO] diffusion curve when subject to inactivation, i.e., NO is scavenged or degraded (Figure 3E, left curve); however, a good fit with the experimental data (Figure 3E, right curve) required potentiation of NO synthesis, which is consistent with the facilitation observed in the paired SSP protocols (Figure 2E). Using physiological levels of spontaneous AP firing, the model predicted basal NO generation and enhanced synthesis with sound-driven activity (Figures S1A

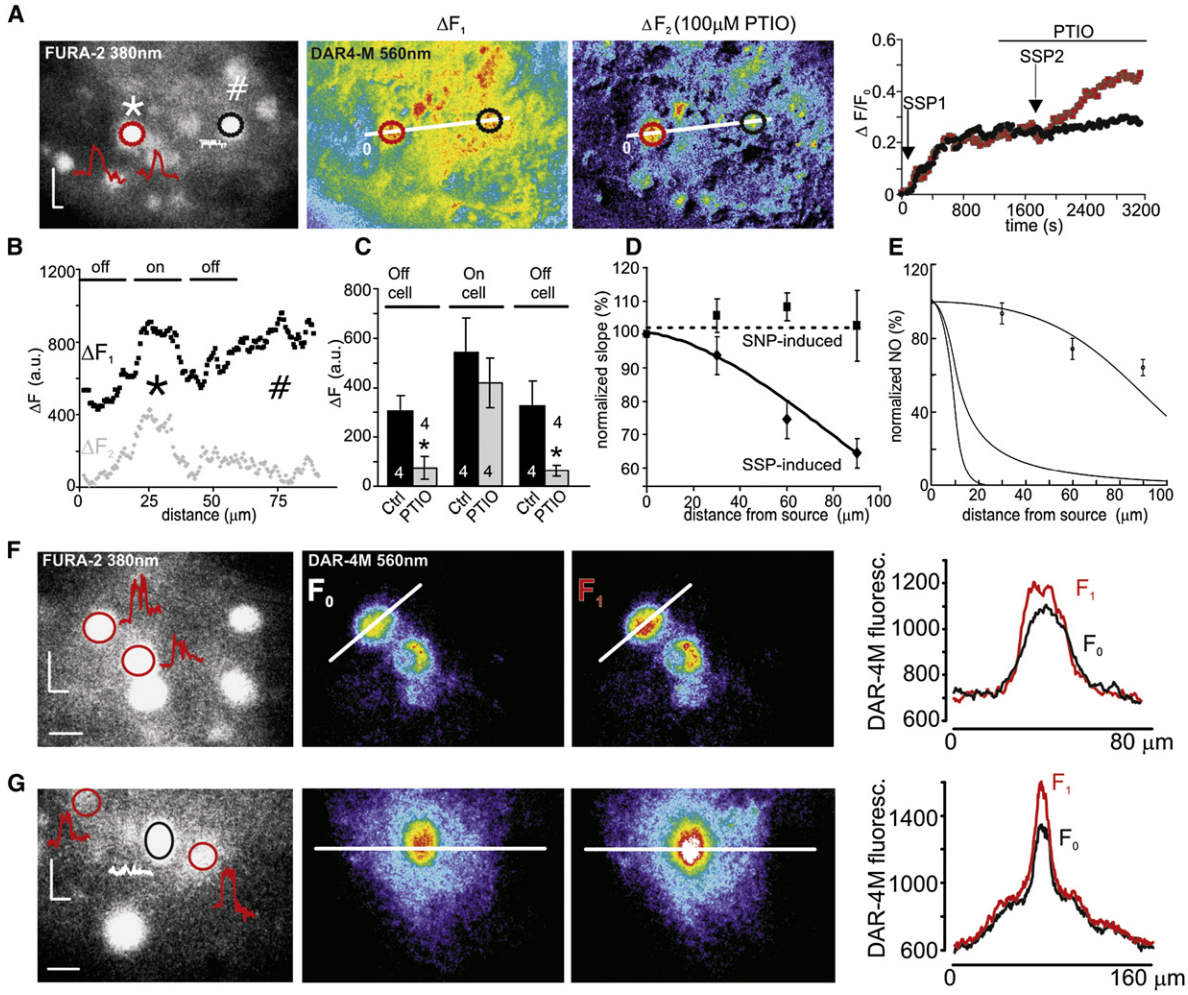

Figure 3. NO Is a Volume Transmitter

(A) NO scavenging isolates the NO rise to connected MNTB neurons alone. Images show Fura-2 fluorescence (left) and SSP-evoked NO fluorescence after SSP1 (ΔF_1) and SSP2 (ΔF_2); the NO scavenger PTIO (100 μM) was applied prior to SSP2. Neuron receiving a calyceal input (*, red circle and trace, 340/380 nm ratio; scale bars, 60 s, 0.04 a.u.), nonconnected neuron (#, black circle and trace, 340/380 nm ratio). Line-scan temporal plot (white line on images, far right graph) shows that PTIO blocks NO accumulation in the nonconnected (black symbols) but not in the connected neuron (red symbols).

(B) A spatial plot of ΔF_1 along a 100 μm line scan from (A). It shows highest NO accumulation in the connected cell (*) and in the neighboring tissue including the nonconnected neuron (#). After PTIO, the ΔF_2 trace (gray) shows reduced fluorescence across the whole slice, except in the connected neuron where synaptic stimulation still induced raised fluorescence.

(C) Summary graph of NO fluorescence in connected MNTB neurons (On cell) and for 20 μm on either side (Off cell) for control (filled bars) and after PTIO (open bars). Student's t test, *$p < 0.05$, means ± SEM, n is indicated within the bars.

(D) The diffusion of NO from connected MNTB neurons is plotted as the change in slope of DAR-4M fluorescence (following an SSP) against distance (diamonds, solid line, n = 7). The slope of responses to NO donor (SNP) perfusion is unchanged with distance (squares, dashed line, n = 7).

(E) Model of NO diffusion from a single 20 μm diameter spherical source (located at distance 0) with a production rate of 800 nM/s. Concentration is normalized to the maximum for the three conditions (from left to right): (1) NO spread by diffusion, with inactivation; (2) diffusion with no inactivation; (3) diffusion and inactivation plus potentiation of NO production as a decaying function of distance from the source center. Circles show data from (D).

(F and G) Same image format as part (A) using labeling of single neurons with Fura-2 and DAR-4M. F_0 is control and F_1 is after SSP stimulation for (F) two connected neurons and (G) one nonconnected neuron located adjacent to two connected neurons. Spatial plots show that NO increases in both cases (F_0 control versus F_1 after SSP; scale bar, 20 μm, all images). All data are means ± SEM.

and S1B), so when the tonotopic distribution of spontaneous activity (Smith et al., 1998) is taken into consideration, the model predicts an in vivo gradient of NO across the tonotopic axis of the MNTB (Figures S1A and S1B), which would interact with tonotopic gradients of ionic conductances measured from "silent" in vitro brain slices (Discussion).

Further confirmation of the volume transmission hypothesis was obtained by loading single neurons with DAR-4M-AM using a loose patch configuration, thus reducing the background fluorescence from the bulk tissue. In one field of view, both labeled cells had intact calyceal inputs (Figure 3F), as indicated by raised intracellular calcium on stimulation (340/380nm ratio traces, red

insets). The line scan across one neuron showed increased fluorescence following synaptic stimulation (F_1) compared to control (F_0). DAR-4M fluorescence is plotted along the line scan for F_0 and F_1 in Figure 3F (right graph). In another experiment, two connected neurons flanked one nonconnected MNTB neuron (Figure 3G). Line scans across the nonconnected neuron showed SSP-evoked rises in DAR-4M fluorescence, as indicated in the example images F_0 (before) and F_1 (after SSP). Similar data were obtained from four such neuron pairs and confirm accumulation of NO in connected as well as in nonconnected neurons following synaptic stimulation.

Nitric Oxide Signaling Suppresses Postsynaptic Kv3 Potassium Currents

Whole-cell patch-clamp recordings from MNTB neurons with an identified calyceal input or from other neurons without a functional input showed that both connected (Figures 4A and 4B, insets show representative traces) and nonconnected neurons (Figures 4D and 4E) had large voltage-activated outward K^+ currents that were suppressed in both cases on synaptic stimulation. The slow 10–15 min time course of the depression (Figures 4B and 4E) was mimicked by perfusion of DEA-NONOate (Figure 4C, open triangles in the absence of stimulation, 100 μM) and contrasts with the minor run-down observed over 20 min recording in slices receiving neither stimulation nor NO donor (Figure 4C, filled squares). Identical results were obtained with SNP (100 μM, n = 6, data not shown), so individual data for SNP and DEA were combined in later figures. Summary data are plotted as mean absolute current magnitude (measured at +50 mV) in Figure 4F, showing the suppression of outward K^+ currents on synaptic stimulation (SSP) by ~50% in connected neurons, which was blocked by perfusion of 1400W (10 μM, n = 4) during the SSP. Similarly, outward potassium currents were suppressed in nonconnected neurons by an SSP and on perfusion of DEA (100 μM). Application of SNP (100 μM) also reduced high-voltage-activated currents (evoked by depolarizations positive to −10 mV, Figure 4G), and this suppression was blocked by the sGC inhibitor 1H-(1,2,4)oxadiazolo[4,3-a]quinozalin-1-one (ODQ, 1 μM) and occluded by perfusion of low concentrations of tetraethylammonium (TEA, 3 mM). This concentration of TEA is selective for Kv3 currents in MNTB neurons (Brew and Forsythe, 2005; Macica et al., 2003) (Figure 4H; summarized in Figure 4I). We conclude that NO is generated in response to stimulation of glutamatergic receptors at the calyx of Held and acts to suppress postsynaptic Kv3 currents within the cell of origin and across a population of active and inactive neurons through a process of volume transmission.

Phosphorylation is a major control mechanism of Kv3 potassium channels (Song et al., 2005); high levels of phosphorylation suppress channel opening, while dephosphorylation increases open probability. Perfusion of the PKG antagonist KT 5823 (1 μM) enhanced resting Kv3 currents and blocked the suppression by SNP. The high-voltage-activated current was confirmed as Kv3 as it was blocked by perfusion with TEA (3 mM) (Figure 4J). In other experiments, the phosphatase inhibitor okadaic acid (100 nM, included in the patch pipette or bath perfused) rapidly suppressed the high-voltage-activated currents (Figure 4K) and occluded the response to NO donors (data not shown). The averaged data are plotted in Figure 4L and suggest that native Kv3 channel activity is highly dependent on the equilibrium between phosphorylation and dephosphorylation. The extent to which this mechanism reflects direct versus indirect actions is presently unclear because of the range of kinase signaling converging at the Kv3.1 channel and needs further investigation.

NO Inhibits Postsynaptic Glutamate Receptors, but Does Not Change Transmitter Release

Volume diffusion of NO between neurons and their synaptic terminals means that the net physiological effect of NO modulation could involve both presynaptic and/or postsynaptic effects. Given the broad spectrum of potential NO actions, we next sought to establish which sites of action were of most relevance for modulation of transmission strength by monitoring the effect of NO donors on MNTB field potentials and by comparing spontaneous and evoked EPSCs at the calyx of Held/MNTB synapse. Perfusion of SNP inhibited the postsynaptic component of the evoked extracellular compound field potentials (Figure S2; C2, postsynaptic) recorded in MNTB following stimulation of the trapezoid body in the brain slice preparation, but it had little or no effect on the presynaptic field potentials (Figure S2; C1, presynaptic) consistent with a postsynaptic mechanism involving reduced synaptic strength, raised firing threshold, and/or reduced excitability.

Kv3 channels are present on both presynaptic and postsynaptic membranes. Suppression of presynaptic Kv3 could potentiate transmitter release, due to increased AP duration and calcium influx (Wang and Kaczmarek, 1998), while suppression of postsynaptic Kv3 would modify postsynaptic MNTB excitability and AP waveform, as shown here. Additionally, NO signaling may exert direct actions on transmitter release or modulate postsynaptic glutamate receptors themselves. Patch-clamp recordings from innervated MNTB neurons exhibited calyceal EPSCs with a mean amplitude of 7.9 nA at the holding potential of −60 mV. NO donors (SNP, 100 μM or DEA, 100 μM) suppressed the evoked AMPAR-mediated EPSCs by 35% ± 4% (n = 7) and slowed the decay kinetics from 0.37 ± 0.07 ms to 0.86 ± 0.2 ms (HP = −60 mV, 37°C, Figures 5A–5D). Similar observations were made for NMDAR-mediated currents with a mean amplitude of 1.8 nA (HP = +50 mV, Figures 5B–5D). The inhibition of both the AMPAR- and NMDAR-mediated EPSCs was mimicked by an SSP, and this was blocked by perfusion with the nNOS antagonist 1400W (10 μM). Although some of these changes could be mediated by either presynaptic or postsynaptic mechanisms, examination of spontaneous miniature EPSCs (mEPSC) in MNTB neurons clearly shows a postsynaptic mechanism. NO donors had no significant effect on release probability, since mEPSC frequencies were unchanged on perfusion of SNP ($f_{control}$ = 7.0 ± 2.9 Hz; f_{NO} = 6.6 ± 3.8 Hz, n = 5). But mEPSC amplitudes were reduced by 27.2% ± 2.3% and their decay kinetics slowed to a similar extent as for evoked EPSCs ($mEPSC_{Control}$ = −73.7 ± 4.8 pA; $mEPSC_{NO}$ = −53.7 ± 4.2 pA; $\tau_{Control}$ = 0.34 ± 0.02 ms; τ_{NO} = 0.51 ± 0.01 ms; HP = −60 mV, $p < 0.05$, paired Student's t test, n = 5; Figures 5E and 5F). Data from the same neuron showed identical changes for evoked EPSCs and mEPSCs on SNP application (inset, Figure 5E). Mean data show comparable

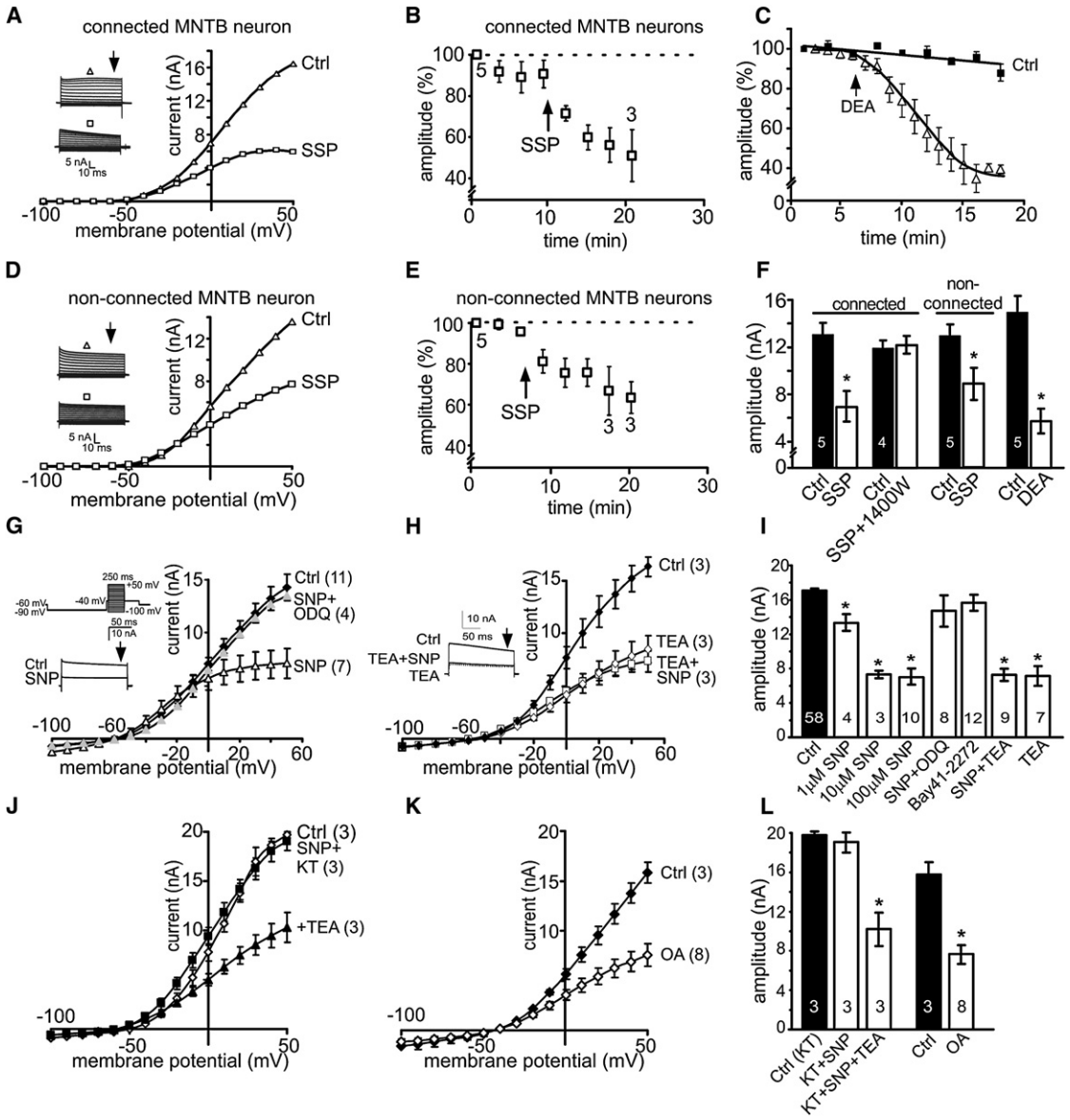

Figure 4. NO Signaling Suppresses Kv3 K^+ Currents in Connected and Nonconnected Neurons

(A) Voltage clamp of outward K^+ currents for an MNTB neuron receiving a calyceal input; leak-subtracted I-V is reduced following an SSP (SSP, open squares); the current recovered after 20 min without stimulation (data not shown). The inset shows representative raw traces.

(B) Time course, the average K^+ current percent amplitude plotted against time for three to five connected MNTB neurons (measured at +50 mV) following SSP stimulation (arrow, numerals indicate cell numbers).

(C) Time course of K^+ current inhibition by DEA-NONOate (100 μM) is similar to SSP-induced depression; plot of percent current amplitude (+50 mV) against time for control (filled symbols, n = 4) and neurons exposed to DEA-NONOate (open symbols, n = 6).

(D) Leak-subtracted I-V relationship for a nonconnected MNTB neuron (same format as [A]). A neighboring connected MNTB neuron (<50 μm away) was stimulated by a SSP; the K^+ currents are reduced in the nonconnected neuron (SSP, open squares).

(E) Average K^+ current amplitude plotted against time for three to five nonconnected MNTB neurons (measured at +50 mV) following SSP stimulation (arrow, numerals indicate cell numbers).

(F) Summary plot of absolute K^+ current amplitude (+50 mV, leak subtracted) following SSP- and DEA-induced K^+ current depression in connected and nonconnected MNTB neurons.

(G) The I-V relationship for outward K^+ currents (filled diamonds, n = 11) is suppressed following perfusion of SNP (100 μM, open triangles). This inhibition was prevented by the sGC inhibitor ODQ (1 μM, gray triangles, n = 4). Inset shows voltage protocol and raw traces at +50 mV with the arrow indicating the measured amplitude plotted in the I-V curve.

(H) Low concentrations of TEA (3 mM) block Kv3 currents (open diamonds, n = 3) after which SNP had no further inhibitory effect (open squares, n = 3), confirming that the NO-modulated current is a Kv3 conductance. Inset shows example current traces.

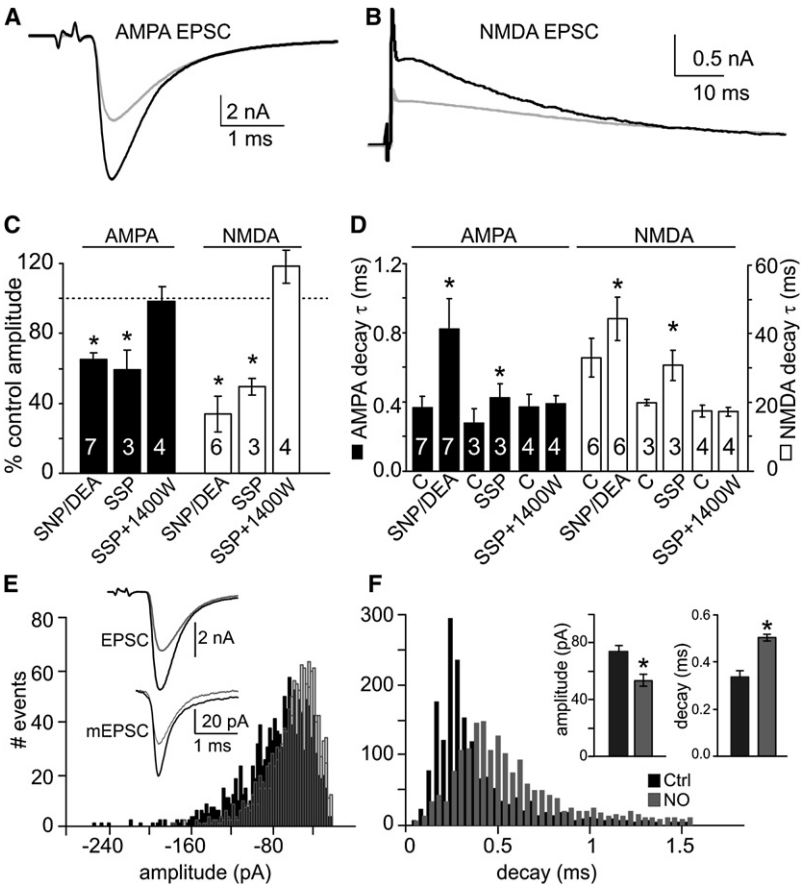

Figure 5. NO Reduces Synaptic Strength by Depressing Postsynaptic AMPAR and NMDAR

(A) Evoked calyceal AMPAR-mediated EPSCs voltage clamped at −60 mV, before (black trace) and after NO donor application (gray trace).

(B) Voltage clamp at +50 mV highlights the slow NMDAR-mediated component, before (black trace) and after NO donor application (gray trace).

(C) AMPAR- (filled bars, −60 mV) and NMDAR-mediated EPSC (open bar, +50 mV) amplitudes are reduced after SNP/DEA (100 μM, DEA was used in two cases) perfusion or SSP application, which was prevented by nNOS inhibition with 1400W (10 μM). Data are expressed as percent control amplitude, with control values being 7.9 ± 1.7 nA and 1.8 ± 0.7 nA, respectively (n = 7).

(D) EPSC decay-time constants for AMPAR- (filled bars) and NMDAR-mediated EPSCs (open bars) were slowed by SNP/DEA or delivery of a SSP and prevented by 1400W (10 μM). Paired Student's t test, *p < 0.05, n is indicated within each bar.

(E) Frequency histogram for mEPSC amplitudes (control, black) and after SNP application (gray, n = 5). Inset shows similar depression of evoked EPSCs and mEPSCs by NO donors from the same cell.

(F) Frequency histogram for control decay-time constants of mEPSCs (black bars) and after SNP application (gray bars, n = 5). Inset shows the mean amplitude and decay changes for both conditions. Paired Student's t test, n = 5, *p < 0.05. All data are means ± SEM, n is indicated by the respective numeral in each case.

significant changes (inset, Figure 5F) and in a further three cases synaptic stimulation with an SSP caused a similar 34.9% ± 11.3% reduction in mEPSC amplitudes. The equivalent depression of amplitude and slowed time course for both miniature and evoked EPSCs is incompatible with a presynaptic mechanism but is consistent with a postsynaptic modulation of AMPAR and NMDAR and is similar to that reported for AMPAR in the hippocampus (Lei et al., 2000). These results confirm that NO has multiple postsynaptic sites of modulatory action: it suppresses postsynaptic Kv3 potassium channels and reduces and slows the evoked calyceal EPSC.

NO Signaling Slows the MNTB Neuron Action Potential

Kv3 channels contribute to AP repolarization in MNTB neurons, so the physiological consequence of their inhibition by endogenous NO should be increased AP half-width. Using current-clamp recording in the whole-cell patch configuration, APs evoked by current injection had half-widths of 0.40 ± 0.01 ms (n = 38), as shown in Figures 6A and 6B. Following 10 min perfusion of SNP or DEA (each 100 μM), AP half-width increased to 0.86 ± 0.07 ms (n = 15). Similarly, physiological stimulation of the calyceal input with an SSP increased AP duration to 0.94 ± 0.08 ms (n = 5). In some cases, an initial increase in AP amplitude was observed at early time points, as would be predicted for a reduction in repolarization conductance. In the presence of 3 mM TEA, which effectively blocks Kv3 channels, half-widths were 0.71 ± 0.13 ms (n = 7), and SNP had no additional effect. Inhibition of nNOS with 1400W or of sGC with ODQ blocked the increase in AP duration by SSP or SNP, with half-widths remaining unchanged at 0.47 ± 0.04 ms (n = 8) and 0.39 ± 0.01 ms (n = 3), respectively.

Confirmation of the ionic mechanisms of these changes in AP waveform were obtained by using a single-compartment MNTB model incorporating Hodgkin-Huxley-type ion channels (see

(I) Summary of K^+ current data shows that SNP dose-dependently reduced Kv3 currents and this was prevented by the sGC antagonist ODQ. The sGC stimulator Bay 41-2272 was without any basal effect. TEA had no additional effect following SNP application.

(J) PKG antagonist KT5823 enhances control outward currents (open diamonds, n = 3), and in its presence, SNP (filled squares) has no effect, even though Kv3 currents are present until blocked by TEA (3 mM, filled triangles, n = 3).

(K) The phosphatase blocker okadaic acid (0.1 μM, filled diamonds) mimics the action of NO signaling by suppressing outward potassium currents relative to control currents (filled diamonds, n = 3).

(L) Summary bar graph shows that KT5823 prevents current suppression by SNP, whereas OA mimics suppression of Kv3 currents. ANOVA was used for significance testing, *p < 0.05, data are means ± SEM, n is indicated by the respective numeral in each case.

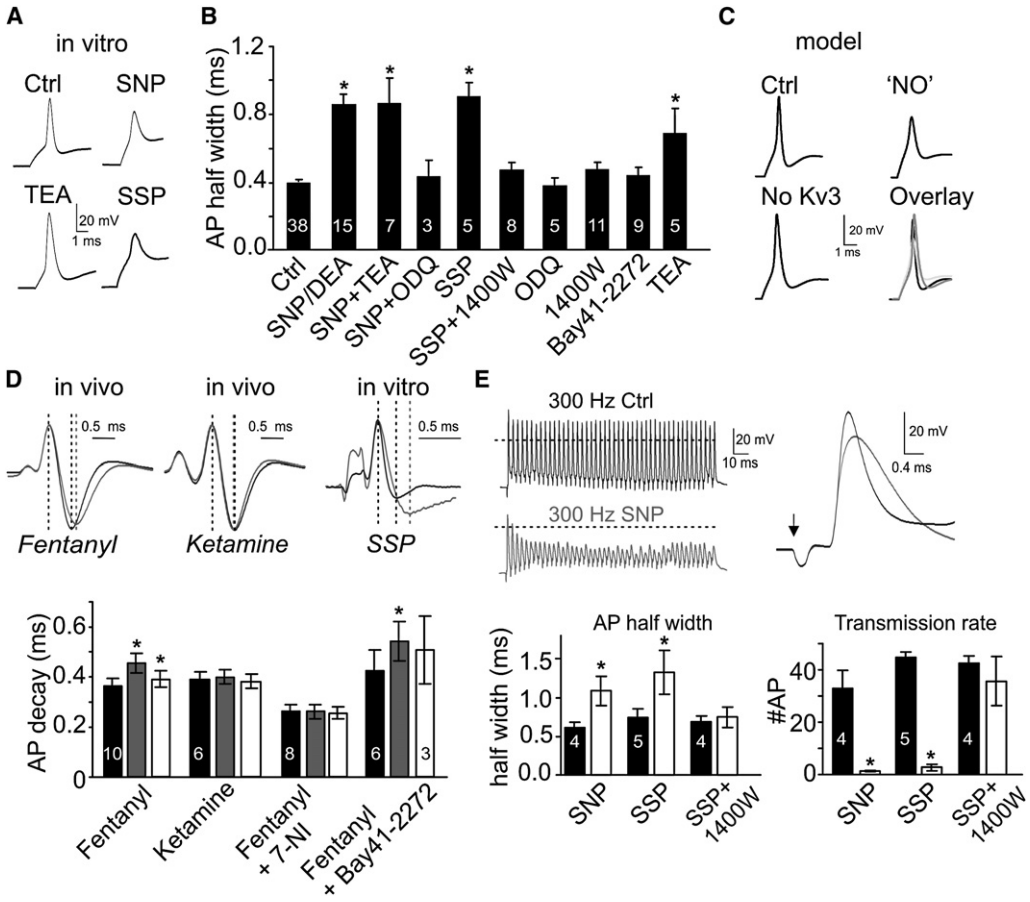

Figure 6. NO Induces Activity-Dependent Changes of Excitability, AP Waveform, and Transmission

(A) Suppression of Kv3 currents prolongs AP duration; similar changes were caused by TEA (3 mM), SNP (100 μM), or a SSP.

(B) Summary of pharmacological data for AP half-widths. NO donors (SNP and DEA; DEA was used in four cases) and TEA slow AP duration. NO-mediated modulation was prevented by ODQ (1 μM), but ODQ or Bay 41-2272 (1 μM) were without effect when applied alone. Synaptic stimulation (SSP) led to similar increases of AP half-width, and this was blocked by 1400W (10 μM); ANOVA, *$p < 0.05$.

(C) Identical AP changes are reproduced in a single-compartment MNTB model incorporating Hodgkin Huxley-type ion channels (see Experimental Procedures) in response to a depolarizing current injection ("control" and "No Kv3," 200 pA; "NO," 250 pA).

(D) Sound-evoked slowing of AP repolarization was observed in mouse MNTB in vivo. Control average AP waveforms (black) from single cells were recorded from mice with anesthetic including fentanyl (left) or ketamine (middle). Immediately after the end of 10–30 min of sound exposure, APs decayed more slowly in fentanyl (gray traces), but did not change with ketamine anesthesia. Right traces show similar slowed AP decay from an in vitro MNTB neuron extracellular potential recording before (black) and after SSP (gray). The summary graph shows in vivo AP decay times for each of four conditions; under control (black bars), at the end of the sound stimulation (gray bars) and immediately following cessation of sound exposure (open bars): (1) fentanyl anesthesia, (2) ketamine anesthesia, (3) fentanyl plus NOS antagonist 7-NI (100 mg/kg, i.p.), which caused shorter MNTB APs and blocked sound-induced AP changes; (4) activation of local sGC by iontophoresis of Bay 41-2272 slowed AP decay under control conditions and during sound exposure; ANOVA, *$p < 0.05$.

(E) Trains of synaptically induced APs (300 Hz, 150 ms) recorded under current-clamp from a MNTB neuron in vitro (black trace). NO donor perfusion (gray trace) and synaptic stimulation (SSP, data not shown) caused a failure of APs after the initial stimulus in each train, with only EPSPs remaining (also see Figure 8). The half-width of the first AP was increased by SNP (100 μM, gray trace, right inset). The graphs summarize the increase in AP half-width and reduced transmission rate following NO donor application or synaptic stimulation (SSP). The SSP-induced changes were blocked by 1400W (10 μM). All data are means ± SEM; significance was assessed by paired Student's t test, *$p < 0.05$, n is indicated by the respective numeral in each case.

Experimental Procedures) in which APs were evoked by depolarizing current injection (200–250 pA). Block of Kv3 currents was simulated by removal of the high-voltage-activated (Kv3) current (Figure 6C, lower left). Interestingly, reproduction of the slowed AP waveform and decreased amplitude caused by NO, required the additional suppression of the voltage-gated Na^+ current by 43% (Figure 6C, top right). Whole-cell patch-clamp recordings of voltage-gated Na^+ currents confirmed that NO donors (SNP and DEA) and delivery of an SSP suppressed the postsynaptic peak voltage-gated Na^+ currents by 37% ± 10% and 50% ± 10%, respectively (Figure S3). Suppression of Na^+ currents was prevented by sGC and nNOS inhibition and was absent in KN2 mice (Gyurko et al., 2002) as shown in Figure S3B. Together these data suggest that NO modulation acts synergistically at multiple sites to modify transmission at this synapse.

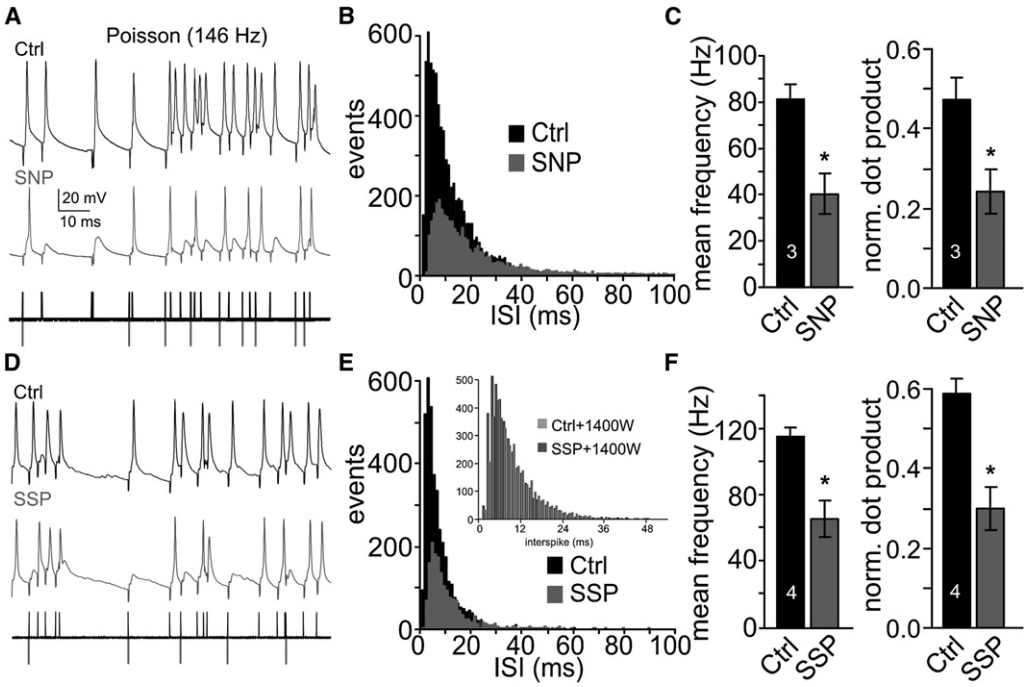

Figure 7. NO Signaling Reduces Spike Train Correlation for Pre- to Postsynaptic Transmission

(A) Current clamp from an MNTB neuron receiving a 146 Hz synaptic stimulus train with Poisson distributed interstimulus intervals (ISI) for control (black) and following SNP application (gray). The lower trace gives an absolute notation of which EPSCs were suprathreshold and generated a postsynaptic AP to the same Poisson train under control (black) and after SNP (gray).

(B) Frequency histogram of ISIs for control (black) and SNP (100 μM, gray) for three neurons receiving a 146 Hz Poisson train.

(C) (Left) Summary of mean postsynaptic AP frequencies; (right) summary of the spike train correlations (normalized dot product, see Experimental Procedures) for control (black) and on SNP application (gray).

(D) Current-clamp data from an MNTB neuron receiving a 146 Hz synaptic stimulus train with Poisson distributed ISIs for control (black) and after SSP application (gray).

(E) Frequency histogram of ISI for control (black) and SSP (gray) for three neurons. Inset shows histogram for one cell incubated with 1400W where a SSP failed to induce failures at higher frequencies.

(F) (Left) Summary of mean postsynaptic AP frequencies; (right) summary of spike train correlations (normalized dot product, see Experimental Procedures) for control (black) and on SSP application (gray). Paired Student's t test, *$p < 0.05$, means ± SEM, n is indicated within each bar.

The Physiological Consequences of NO Generation, In Vitro and In Vivo

The in vitro results suggest that modest levels of auditory activity should influence AP firing and hence information transmission across this relay synapse. To test for this, we recorded from mouse MNTB in vivo and compared sound-evoked unitary AP waveforms under ketamine anesthesia (in which NMDAR are blocked and nNOS activity suppressed) with equivalent recordings under fentanyl anethesia (Figure 6D), an anesthetic that does not block NMDAR. In ketamine-anesthetized animals, sound exposure induced no change in AP waveform. Sound-evoked activity (10–30 min) induced a slowing of AP repolarization in fentanyl-anesthetized mice, which was maintained after ceasing sound exposure. This sound-induced change in AP time course could be blocked by administration of the nNOS antagonist 7-nitroindazole (7-NI, 100 mg/kg, i.p.) and potentiated by local iontophoretic application of Bay 41-2272 (Figure 6D). In one case where prespikes (corresponding to calyceal APs) were observed with use of an iontophoretic pipette, application of Bay 41-2272 increased failures of postsynaptic AP firing, consistent with the in vitro observations in Figure 7. Similar AP waveforms were obtained for extracellular recordings from single MNTB neurons in slice preparations after SSP application (Figure 6D, right, scaled traces: control in black and SSP in gray). A SSP increased AP waveform decay from 0.38 ± 0.11 ms to 0.53 ± 0.16 ms ($n = 4$, $p = 0.042$, paired Student's t test). These results are consistent with mediation of sound activity-dependent change in AP waveform through a signaling cascade involving NMDAR, nNOS, and sGC to modulate Kv3 currents, as predicted from the in vitro data.

To determine the physiological consequences of this NO signaling, we examined synaptically evoked 300 Hz trains lasting 150 ms under current-clamp recording conditions (Figure 6E). SNP increased the AP half-widths (Figure 6E) as observed above and reduced transmission rate, as estimated by the number of APs reaching threshold (dotted line). Furthermore, when neurons were stimulated by a SSP, AP half-width increased and transmission started to fail, similar to that seen for application of a NO donor. These failures were abolished by the NOS inhibitor (1400W, 10 μM, Figure 6E), confirming the involvement of endogenous

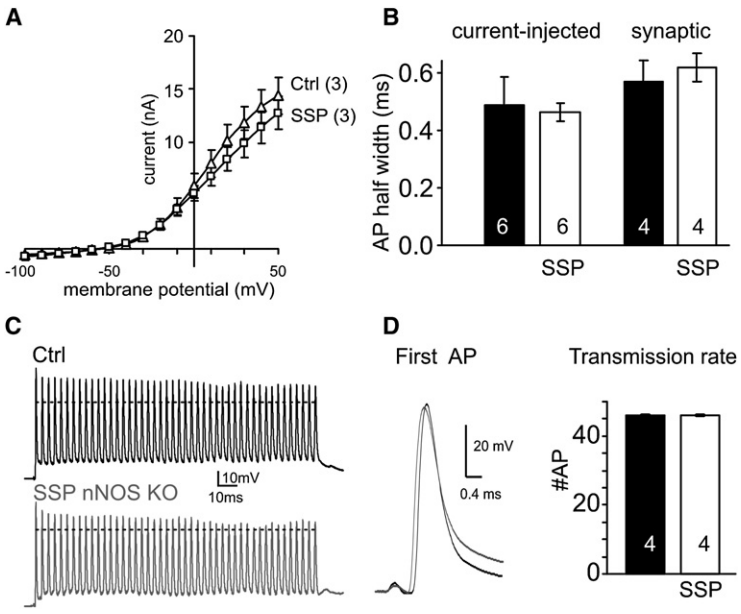

Figure 8. Activity-Dependent Changes Are Absent in a nNOS Knockout Mouse

(A) I-V relationship of outward currents in MNTB neurons from nNOS exon 6 knockout (KN2) mice. Synaptic stimulation (SSP) caused no change in high-voltage-activated currents.

(B) Mean half-widths of APs (control, black bars) induced by current injection or by synaptic stimulation (SSP, open bars) are unchanged after a SSP.

(C) Trains of synaptically induced APs (300 Hz, 150 ms) recorded under current clamp in an MNTB neuron from a KN2 mouse (Ctrl, upper black trace) is similar to the controls from normal mice, but synaptic stimulation (SSP, lower gray trace) had no effect.

(D) The first AP of the train for both conditions is superimposed (middle traces) and shows no difference in the half-width following an SSP. The transmission rate was also unaffected by administering an SSP (right bar graph). All data are means ± SEM, n is indicated by the respective numeral in each case.

release and action of NO. Thus, the response of the MNTB neuron to the 300 Hz stimulation changed from tonic firing to an onset or phasic response and vastly reduced the efficacy of transmission across the calyx of Held/MNTB synapse from 100% transmission (input:output AP) in control conditions to 4.7% ± 1.6% (300 Hz train, Figure 6E, bottom graph) following NO signaling.

This change will have a dramatic influence on transmission of information across the MNTB by shifting the output firing from 1:1 following the presynaptic firing pattern to a phasic onset response. Synaptically evoked trains with Poisson-distributed interspike intervals (ISI, mean frequency 146 Hz) showed mean transmission rates of 82.1 ± 5.5 Hz under control conditions (Figure 7A), which decreased to 38.5 ± 7.9 Hz on perfusion of SNP (Figure 7A). The frequency histogram (Figure 7B) shows strongly reduced AP firing following ISIs shorter than 21 ms, whereas AP firing following longer ISIs was unchanged. In line with the decreased firing frequency, the correlation between the input stimulus train and the output AP train is reduced from 0.47 ± 0.05 to 0.24 ± 0.06 ($p < 0.05$, paired Students t test, $n = 3$) following SNP and measured by the product of spike vectors (Figure 7C, right; see Experimental Procedures). Identical changes were observed on activating endogenous NO signaling with a SSP stimulation (Figures 7D–7F), and this was inhibited by simultaneous perfusion of the nNOS antagonist 1400W (10 μM, inset Figure 7E).

Activity-Dependent Modulation of Kv3 Current Is Absent in an nNOS Knockout Mouse

We reasoned that if this activity-dependent signaling were mediated by NO, modulation of Kv3 and AP waveform should be absent in an nNOS knockout mouse. Whole-cell patch recordings were made from five MNTB neurons receiving calyceal inputs in brain slices from the KN2 mouse (Gyurko et al., 2002). The synaptic inputs were of similar magnitude to control animals (10.9 ± 1.1 nA, −60 mV, n = 5, data not shown). Outward potassium currents were also of similar magnitude to normal animals (Figure 8A, open triangles) and were sensitive to 3 mM TEA (data not shown). The outward current was unaffected by delivery of a SSP (open squares), and no change was observed in AP half-width following a SSP (Figure 8B). Furthermore, delivery of short synaptic trains (300 Hz, 150 ms) always generated postsynaptic APs, and this too was unaffected by a prior SSP (Figure 8C). In one case, application of an NO-donor after a negative SSP response, suppressed outward K^+ currents, EPSCs, and broaden AP half-width, confirming that downstream components of the signaling pathway were otherwise intact in the KO animal.

DISCUSSION

These results demonstrate that nitric oxide is an endogenous activity-dependent regulator of neuronal excitability and is predominantly mediated by changes in phosphorylation of postsynaptic Kv3 potassium channels, although several other targets are also involved. The data show that nNOS is activated by NMDAR at the calyx of Held. NO acts via sGC to raise cGMP and alters the balance between phosphorylation and dephosphorylation of Kv3 channels: dominance of kinase signaling inhibits Kv3, while supremacy of phosphatase signaling enhances Kv3 currents. Kv3 is closely associated with AP repolarization, so suppression leads to longer APs, more sustained depolarization, and inactivation of voltage-gated sodium channels, hence reducing gain and information transmission. The results are consistent with NO acting as a nonclassical neurotransmitter or volume transmitter, in that modulation is induced in local inactive neurons by diffusion from adjacent active neurons and suggests that NO signaling scales postsynaptic excitability to changes in synaptic activity across a population of neurons.

There is increasing evidence for nonclassical forms of synaptic transmission in the brain (Bullock et al., 2005), ranging from "spill-over" of neurotransmitter in the synaptic cleft (DiGregorio et al., 2002) to longer-range diffusion, including neuronal-glia interactions, of catecholamine, peptidergic, purinergic, and cannabinoid transmitters (Carlson et al., 2002; Fields and Burnstock, 2006). The concept of volume transmission is increasingly recognized as an integral part of brain function (Fuxe et al., 2007). NO is commonly highlighted as possessing the attributes

required of a volume transmitter, but the distributed inputs of most excitatory synapses have made this difficult to prove.

Many studies of nitrergic physiology in the brain have focused on changes in synaptic strength, but here we show that this is only part of the mechanism and that postsynaptic excitability changes are also important. NO is acting at multiple sites: locally at glutamate receptors and ionic conductances within the innervated neuron and also by diffusion to adjacent cells. Our data are consistent with tight coupling of NMDAR to nNOS via Ca^{2+} influx, although contributions from Ca^{2+}-permeable AMPAR are possible. There is also a well-documented decline in the magnitude of NMDAR currents during maturation at the endbulb and calyx of Held (Bellingham et al., 1998; Futai et al., 2001; Joshi and Wang, 2002). Previously, this has been extrapolated to suggest the absence of functional NMDARs at mature brainstem synapses and so it could be argued that coupling to nNOS may be dominated by Ca^{2+}-permeable AMPAR on maturation. However, this is incompatible with block of the in vivo AP changes by ketamine and with data from P21 mice, where the SSP-induced DAR-4M fluorescence signals (indicating NO generation) were completely suppressed by the NMDAR antagonist AP-5 (Figure S4B). Two further observations confirm the primacy of NMDARs in coupling to nNOS: first, although NMDARs decline, they are not eradicated, and their slow kinetics means that in terms of conductance (integral) they dominate calyceal AMPARs by 5:1 (Figure S4A) and summate during repetitive stimulation. Second, we have confirmed synaptic NMDAR-mediated currents in P35 mice (Figure S4C) and provided temporal overlap between in vitro and in vivo recordings from the MNTB (animal ages of P10–P35 and P17–P70, respectively). Finally, it might be argued that the NMDARs are functionally inert due to voltage-dependent block by Mg^{2+} at resting membrane potentials. However the SSP and sound-evoked stimuli generate AP trains, each AP will relieve the voltage-dependent block, allowing a pulse of calcium influx (Bollmann et al., 1998; Spruston et al., 1995). Together these results strongly suggest that NMDAR are functionally relevant at mature calyceal synapses and preserve tight coupling to nNOS, presumably through their mutual PDZ-binding domains (Kornau et al., 1995). Finally, the in vivo data show that anesthetic doses of ketamine largely suppress NMDAR (Binns and Salt, 1995) and hence NO signaling.

The broad range of targets raises the possibility that multiple signaling pathways could be involved. We can exclude major contributions from cannabinoid (Kushmerick et al., 2004), metabotropic glutamate receptors (Billups et al., 2005), and A1 adenosine receptors (Wong et al., 2006) since antagonists for these receptors had no effect on Kv3 suppression by a SSP (data not shown). Further evidence supporting the predominance of NO signaling is that modulation of Kv3 currents and AP waveforms were absent from the KN2 nNOS knockout mice (Gyurko et al., 2002). The evidence for endogenous NO generation following synaptic stimulation and its action in modulating local and distant neurons constitutes strong evidence that NO is a volume transmitter in the auditory pathway. We postulate that diffusion and summation from multiple sources provides one means of integrating global activity, allowing a slow time course equilibration between excitability and synaptic transmission across the neuronal population, which would complement

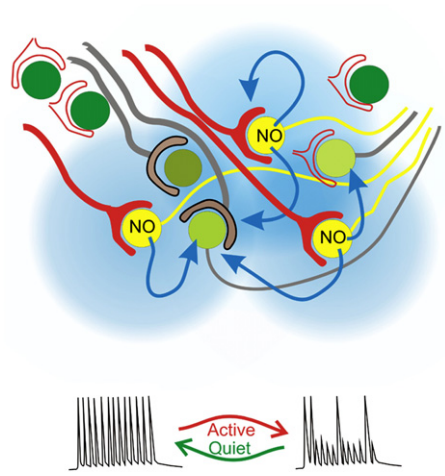

Figure 9. NO Diffusion and Summation across a Population of Active and Inactive Neurons

Diffusion of NO from multiple active sources provides modulatory control of synaptic strength and postsynaptic excitability across a population of active and inactive neurons. Three MNTB neurons are shown with highly active calyceal inputs (red), driving these cells to be strong NO sources. This NO can diffuse to influence presynaptic terminals and inactive MNTB neurons in the vicinity. Summation of NO from multiple sources and including spontaneous and evoked activity provides a volume transmission signaling mechanism.

cell-autonomous mechanisms of synaptic plasticity. This concept is illustrated in Figure 9, in which NO generation by active MNTB neurons summates and modulates excitability across active and inactive cells. Differences in activity rates (including spontaneous firing) across the nucleus could act to adjust the functional tonotopic gradients of intrinsic conductances, which have been previously documented (Brew and Forsythe, 2005; Smith et al., 1998; Wang et al., 1998). For instance, the highest spontaneous firing is observed in medial neurons receiving information on high sound frequencies, they exhibit the largest Kv3 currents, but we now predict that they are under the greatest suppression by NO (as illustrated by the NO diffusion model, Figure S1) so the functional Kv3 current in vivo will be less than that measured from in vitro quiescent slices.

The modulation of both voltage-gated K^+ and Na^+ conductances downstream of activity-dependent NO generation suggests contributions to intrinsic excitability (Daoudal and Debanne, 2003) and/or homeostatic scaling (Marder and Prinz, 2002), with levels of spontaneous activity in the auditory pathway sustaining "basal" nNOS activity over long periods. Short-term modulation (milliseconds to seconds) at the calyx arises from biophysical phenomena (e.g., facilitation, short-term depression, posttetanic potentiation, and vesicle recycling [von Gersdorff and Borst, 2002]), which is highly dependent on the recent history and ongoing activity (including spontaneous activity) as recently described by Hermann et al. (2007). This is distinct from the NO signaling studied here, which has a much slower time course so that with activation by spontaneous firing, modulation is extended to indefinite timescales. Phosphorylation of Kv3.1b at Ser-503 (Song et al., 2005) is unlikely to mediate this NO-mediated modulation, since this site is not present in mouse *kcnc1*, but NO-mediated suppression of recombinant Kv3

channels has been observed via a PKG/phosphatase-dependent mechanism (Moreno et al., 2001). These results are of general application since Kv3 K^+ channels and nNOS are broadly expressed throughout the central nervous system and there is significant colocalization; for example, in the hippocampus, 86% of nNOS-expressing interneurons also express Kv3 subunits (Tansey et al., 2002).

Since brain slices are isolated and inactive for several hours before recording, it seems likely that MNTB basal properties will differ from in vivo recordings where neurons are continually exposed to ongoing spontaneous activity. The lack of spontaneous activity in vitro means that NO modulation will be low and Kv3 currents larger in these quiescent slices than under physiological conditions. The Poisson-distributed stimulation paradigm shows that high transmission rates (>50 Hz) are most strongly suppressed (while onset responses and firing at frequencies below 50 Hz are largely unaffected). Transmission failure is consistent with in vivo MNTB recordings during sound stimulation where failures are observed (Kopp-Scheinpflug et al., 2003) and responses to sound show "primary-like" poststimulus time histograms. In terms of brainstem auditory function, NO signaling will have little impact on onset responses but will reduce firing rates of MNTB neurons during sustained activity. We do not yet know whether NO modulates cochlear nucleus or upstream nuclei in the SOC and inferior colliculus, so the net effect of NO signaling on hearing may be complex and will require further investigation.

Together, these results show that nitric oxide plays an important role in balancing presynaptic activity with postsynaptic excitability, perhaps serving as a slow gain-control mechanism. We conclude that NO is an activity-dependent volume modulator, adapting intrinsic excitability and synaptic efficacy and modulating both active and inactive neuronal populations to the same physiological input.

EXPERIMENTAL PROCEDURES

In Vitro Preparations

CBA/CaJ and KN2 (Gyurko et al., 2002) mice aged P10–P35 were killed by decapitation in accordance with the UK Animals (Scientific Procedures) Act 1986, and brainstem slices containing the superior olivary complex (SOC) were prepared as previously described (Barnes-Davies and Forsythe, 1995). Transverse slices (200 μm thick) containing the MNTB were cut in a low-sodium artificial CSF (aCSF) at ~0°C. Slices were maintained in a normal aCSF at 37°C for 1 hr, after which they were stored at room temperature (~20°C). Composition of the normal aCSF was (in mM) as follows: NaCl 125, KCl 2.5, $NaHCO_3$ 26, glucose 10, NaH_2PO_4 1.25, sodium pyruvate 2, myo-inositol 3, $CaCl_2$ 2, $MgCl_2$ 1, and ascorbic acid 0.5; L-arginine 0.1; pH was 7.4, bubbled with 95% O_2, 5% CO_2. For the low-sodium aCSF, NaCl was replaced by 250 mM sucrose, and $CaCl_2$ and $MgCl_2$ concentrations were changed to 0.1 and 4 mM, respectively. All experiments were carried out at 36°C ± 1°C using feedback control of a Peltier device warming the perfusing aCSF (1 ml/min).

Electrophysiology

Patch Clamp

Whole-cell patch-clamp recordings were made from visually identified MNTB neurons (microscope: Nikon E600FN with DIC optics) using a Multiclamp 700B amplifier and pClamp 9 software (Molecular Devices, Sunnyvale, CA, USA) sampling at 50 kHz and filtering at 10 kHz. Patch pipettes were pulled from borosilicate glass capillaries (GC150F-7.5, OD: 1.5 mm; Harvard Apparatus, Edenbridge, UK) using a two-stage vertical puller (PC-10 Narishige, Tokyo, Japan). Their resistance was ~3.0 MΩ when filled with a patch solution containing the following (in mM): KCl 110, HEPES 40, EGTA 0.2, $MgCl_2$ 1, $CaCl_2$ 0.1, Na_2phosphocreatine 5, L-arginine 1; pH was adjusted to 7.2 with KOH and 2 mM ATP and 0.5 mM GTP were added on the day of use. Whole-cell series resistances were <12 MΩ, compensated by 70%.

Synaptic Stimulation

EPSCs were evoked with a bipolar platinum electrode placed at the midline and using a DS2A isolated stimulator (~3–8 V, 0.2 ms; Digitimer, Welwyn Garden City, UK). Synaptic connections were detected using a Fura2 AM (Molecular Probes, Eugene, OR, USA) imaging technique described previously (Billups et al., 2002).

Imaging

Imaging was conducted using a PentaMax intensified CCD camera (Princeton Instruments, Inc). The fluorescent image (emission >505 nm) was displayed using Metafluor imaging software (Series 7, Molecular Devices), the light source was a Polychrome II Monochromator (TILL Photonics, Martinsried, Germany). For loading of DAR-4M, slices were incubated for 30 min in 5 ml of 10 μM DAR-4M AM at room temperature. After loading, slices were postincubated in aCSF for 30 min and then transferred to the recording chamber. For measurements of NO production, DAR-4M was excited at 560 nm and images acquired every 5 s (exposure time: 20 ms) (Mottola et al., 2005). The fluorescence above 575 nm was detected using an IF excitation filter, a DM550 dichroic mirror, and a BA575 emission filter (Nikon, Tokyo, Japan).

Radio-Immunoassay of Cyclic GMP

Radio-immunoassay of cyclic GMP was conducted in identical slices to the electrophysiology and imaging (see Supplemental Experimental Procedures).

In Vivo Recordings

Spontaneous and evoked responses were recorded from mice (C3HeB/FeJ) MNTB neurons (P17–P70). During the surgical preparation, the animals were anesthetized with a mixture of ketamine hydrochloride (100 mg/kg BW) and xylazine hydrochloride (5 mg/kg BW). In a subset of experiments, the surgical preparation was done under ketamine anesthesia while the electrophysiological recordings were performed using a mixture of fentanyl (0.05 mg/kg), medetomidin (0.5 mg/kg), and xylazine hydrochloride (5 mg/kg). Extracellular recordings were made using glass pipettes filled with 3 M KCl. MNTB single-unit recordings characteristically possess a prepotential, followed by a biphasic postsynaptic action potential and responded to sound from the contralateral ear only (Kopp-Scheinpflug et al., 2008).

Immunohistochemistry

Immunohistochemistry was conducted on 12 μm cryostat sections fixed in either methanol or 4% PFA and processed using standard procedures detailed in the Supplemental Experimental Procedures. Antibody sources and details are presented in Table S1.

Action Potential Modeling

A single compartment model of an MNTB principal neuron was constructed using the NEURON simulation software (Carnevale and Lebeda, 1987) by adapting a type II ventral cochlea nucleus cell model (Rothman and Manis, 2003). The MNTB model contained a voltage-gated Na^+ current, a low-voltage activated K^+ current, a high-voltage activated K^+ current (Kv3), a hyperpolarization-activated current (I_h), and a leak current. The magnitudes and reversal potentials of the conductances and the model parameters are given in Table S2.

Mathematical Modeling of NO Diffusion

The spread of NO within a block of neural tissue was considered in two different cases: (1) 20 μm diameter spherical source of NO located within a large spherical block of tissue and (2) an array of sources in a rectangular slab of tissue. Sources produce NO at a constant rate. NO dissipates by diffusion and is subject to inactivation. Production, diffusion, and inactivation rates are as per Hall and Garthwaite (2006). Numerical simulations were carried out in MATLAB, details are in the Supplemental Experimental Procedures and source code is available from the author (b.graham@cs.stir.ac.uk).

Data Analysis and Statistical Methods

Results are reported as mean ± SEM. Statistical comparison was carried out using Student's t test (paired or unpaired and one- or two-tailed, as indicated), and one-way ANOVA was applied when comparing more than two data sets. Differences were considered statistically significant at $p < 0.05$.

SUPPLEMENTAL DATA

The Supplemental Data include figures and Experimental Procedures and can be found with this article online at http://www.neuron.org/supplemental/S0896-6273(08)00758-7.

ACKNOWLEDGMENTS

Thanks to Volko Straub for comments on a draft manuscript. We are grateful to Paul L. Huang for the generous provision of KN2 transgenic mice. This work was supported by the following organizations: Medical Research Council, Deutsche Forschungsgemeinschaft (Ru 390/18-1), Biotechnology and Biological Sciences Research Council, and Deafness Research UK.

Accepted: August 29, 2008
Published: November 25, 2008

REFERENCES

Ahern, G.P., Klyachko, V.A., and Jackson, M.B. (2002). cGMP and S-nitrosylation: two routes for modulation of neuronal excitability by NO. Trends Neurosci. *25*, 510–517.

Barnes-Davies, M., and Forsythe, I.D. (1995). Pre- and postsynaptic glutamate receptors at a giant excitatory synapse in rat auditory brainstem slices. J. Physiol. *488*, 387–406.

Bellingham, M.C., Lim, R., and Walmsley, B. (1998). Developmental changes in EPSC quantal size and quantal content at a central glutamatergic synapse in rat. J. Physiol. *511*, 861–869.

Billups, B. (2005). Colocalization of vesicular glutamate transporters in the rat superior olivary complex. Neurosci. Lett. *382*, 66–70.

Billups, B., Wong, A.Y., and Forsythe, I.D. (2002). Detecting synaptic connections in the medial nucleus of the trapezoid body using calcium imaging. Pflugers Arch. *444*, 663–669.

Billups, B., Graham, B.P., Wong, A.Y., and Forsythe, I.D. (2005). Unmasking group III metabotropic glutamate autoreceptor function at excitatory synapses in the rat CNS. J. Physiol. *565*, 885–896.

Binns, K.E., and Salt, T.E. (1995). Excitatory amino acid receptors modulate habituation of the response to visual stimulation in the cat superior colliculus. Vis. Neurosci. *12*, 563–571.

Bogdan, C. (2001). Nitric oxide and the immune response. Nat. Immunol. *2*, 907–916.

Bollmann, J.H., Helmchen, F., Borst, J.G., and Sakmann, B. (1998). Postsynaptic Ca^{2+} influx mediated by three different pathways during synaptic transmission at a calyx-type synapse. J. Neurosci. *18*, 10409–10419.

Bon, C.L., and Garthwaite, J. (2003). On the role of nitric oxide in hippocampal long-term potentiation. J. Neurosci. *23*, 1941–1948.

Bredt, D.S., Hwang, P.M., and Snyder, S.H. (1990). Localization of nitric oxide synthase indicating a neural role for nitric oxide. Nature *347*, 768–770.

Brenman, J.E., Chao, D.S., Gee, S.H., McGee, A.W., Craven, S.E., Santillano, D.R., Wu, Z., Huang, F., Xia, H., Peters, M.F., et al. (1996). Interaction of nitric oxide synthase with the postsynaptic density protein PSD-95 and alpha1-syntrophin mediated by PDZ domains. Cell *84*, 757–767.

Brew, H.M., and Forsythe, I.D. (2005). Systematic variation of potassium current amplitudes across the tonotopic axis of the rat medial nucleus of the trapezoid body. Hear. Res. *206*, 116–132.

Bullock, T.H., Bennett, M.V., Johnston, D., Josephson, R., Marder, E., and Fields, R.D. (2005). Neuroscience. The neuron doctrine, redux. Science *310*, 791–793.

Carlson, G., Wang, Y., and Alger, B.E. (2002). Endocannabinoids facilitate the induction of LTP in the hippocampus. Nat. Neurosci. *5*, 723–724.

Carnevale, N.T., and Lebeda, F.J. (1987). Numerical analysis of electrotonus in multicompartmental neuron models. J. Neurosci. Methods *19*, 69–87.

Daoudal, G., and Debanne, D. (2003). Long-term plasticity of intrinsic excitability: learning rules and mechanisms. Learn. Mem. *10*, 456–465.

DiGregorio, D.A., Nusser, Z., and Silver, R.A. (2002). Spillover of glutamate onto synaptic AMPA receptors enhances fast transmission at a cerebellar synapse. Neuron *35*, 521–533.

Dodson, P.D., Barker, M.C., and Forsythe, I.D. (2002). Two heteromeric Kv1 potassium channels differentially regulate action potential firing. J. Neurosci. *22*, 6953–6961.

Elezgarai, I., Diez, J., Puente, N., Azkue, J.J., Benitez, R., Bilbao, A., Knopfel, T., Donate-Oliver, F., and Grandes, P. (2003). Subcellular localization of the voltage-dependent potassium channel Kv3.1b in postnatal and adult rat medial nucleus of the trapezoid body. Neuroscience *118*, 889–898.

Fessenden, J.D., Altschuler, R.A., Seasholtz, A.F., and Schacht, J. (1999). Nitric oxide/cyclic guanosine monophosphate pathway in the peripheral and central auditory system of the rat. J. Comp. Neurol. *404*, 52–63.

Fields, R.D., and Burnstock, G. (2006). Purinergic signalling in neuron-glia interactions. Nat. Rev. Neurosci. *7*, 423–436.

Forsythe, I.D. (1994). Direct patch recording from identified presynaptic terminals mediating glutamatergic EPSCs in the rat CNS, in vitro. J. Physiol. *479*, 381–387.

Forsythe, I.D., and Westbrook, G.L. (1988). Slow excitatory postsynaptic currents mediated by N-methyl-D-aspartate receptors on cultured mouse central neurones. J. Physiol. *396*, 515–533.

Futai, K., Okada, M., Matsuyama, K., and Takahashi, T. (2001). High-fidelity transmission acquired via a developmental decrease in NMDA receptor expression at an auditory synapse. J. Neurosci. *21*, 3342–3349.

Fuxe, K., Dahlstrom, A., Hoistad, M., Marcellino, D., Jansson, A., Rivera, A., Diaz-Cabiale, Z., Jacobsen, K., Tinner-Staines, B., Hagman, B., et al. (2007). From the Golgi-Cajal mapping to the transmitter-based characterization of the neuronal networks leading to two modes of brain communication: wiring and volume transmission. Brain Res. Brain Res. Rev. *55*, 17–54.

Garthwaite, J. (2008). Concepts of neural nitric oxide-mediated transmission. Eur. J. Neurosci. *27*, 2783–2802.

Gyurko, R., Leupen, S., and Huang, P.L. (2002). Deletion of exon 6 of the neuronal nitric oxide synthase gene in mice results in hypogonadism and infertility. Endocrinology *143*, 2767–2774.

Hall, C.N., and Garthwaite, J. (2006). Inactivation by nitric oxide by cerebellar slices. J. Physiol. *577*, 549–567.

Hermann, J., Pecka, M., von Gersdorff, H., Grothe, B., and Klug, A. (2007). Synaptic transmission at the calyx of held under in vivo like activity levels. J. Neurophysiol. *98*, 807–820.

Hopper, R.A., and Garthwaite, J. (2006). Tonic and phasic nitric oxide signals in hippocampal long-term potentiation. J. Neurosci. *26*, 11513–11521.

Hurt, K.J., Sezen, S.F., Champion, H.C., Crone, J.K., Palese, M.A., Huang, P.L., Sawa, A., Luo, X., Musicki, B., Snyder, S.H., and Burnett, A.L. (2006). Alternatively spliced neuronal nitric oxide synthase mediates penile erection. Proc. Natl. Acad. Sci. USA *103*, 3440–3443.

Ignarro, L.J., Buga, G.M., Wood, K.S., Byrns, R.E., and Chaudhuri, G. (1987). Endothelium-derived relaxing factor produced and released from artery and vein is nitric oxide. Proc. Natl. Acad. Sci. USA *84*, 9265–9269.

Jacoby, S., Sims, R.E., and Hartell, N.A. (2001). Nitric oxide is required for the induction and heterosynaptic spread of long-term potentiation in rat cerebellar slices. J. Physiol. *535*, 825–839.

Joshi, I., and Wang, L.Y. (2002). Developmental profiles of glutamate receptors and synaptic transmission at a single synapse in the mouse auditory brainstem. J. Physiol. *540*, 861–873.

Joshi, I., Shokralla, S., Titis, P., and Wang, L.Y. (2004). The role of AMPA receptor gating in the development of high-fidelity neurotransmission at the calyx of Held synapse. J. Neurosci. *24*, 183–196.

Kojima, H., Hirotani, M., Nakatsubo, N., Kikuchi, K., Urano, Y., Higuchi, T., Hirata, Y., and Nagano, T. (2001). Bioimaging of nitric oxide with fluorescent indicators based on the rhodamine chromophore. Anal. Chem. *73*, 1967–1973.

Kopp-Scheinpflug, C., Lippe, W.R., Dorrscheidt, G.J., and Rubsamen, R. (2003). The medial nucleus of the trapezoid body in the gerbil is more than a relay: comparison of pre- and postsynaptic activity. J. Assoc. Res. Otolaryngol. *4*, 1–23.

Kopp-Scheinpflug, C., Tolnai, S., Malmierca, M.S., and Rubsamen, R. (2008). The medial nucleus of the trapezoid body: comparative physiology. Neuroscience *154*, 160–170.

Kornau, H.C., Schenker, L.T., Kennedy, M.B., and Seeburg, P.H. (1995). Domain interaction between NMDA receptor subunits and the postsynaptic density protein PSD-95. Science *269*, 1737–1740.

Kushmerick, C., Price, G.D., Taschenberger, H., Puente, N., Renden, R., Wadiche, J.I., Duvoisin, R.M., Grandes, P., and von Gersdorff, H. (2004). Retroinhibition of presynaptic Ca^{2+} currents by endocannabinoids released via postsynaptic mGluR activation at a calyx synapse. J. Neurosci. *24*, 5955–5965.

Lei, S., Jackson, M.F., Jia, Z., Roder, J., Bai, D., Orser, B.A., and MacDonald, J.F. (2000). Cyclic GMP-dependent feedback inhibition of AMPA receptors is independent of PKG. Nat. Neurosci. *3*, 559–565.

Lein, E.S., Hawrylycz, M.J., Ao, N., Ayres, M., Bensinger, A., Bernard, A., Boe, A.F., Boguski, M.S., Brockway, K.S., Byrnes, E.J., et al. (2007). Genome-wide atlas of gene expression in the adult mouse brain. Nature *445*, 168–176.

Liberman, M.C., and Oliver, M.E. (1984). Morphometry of intracellularly labeled neurons of the auditory nerve: correlations with functional properties. J. Comp. Neurol. *223*, 163–176.

Macica, C.M., von Hehn, C.A., Wang, L.Y., Ho, C.S., Yokoyama, S., Joho, R.H., and Kaczmarek, L.K. (2003). Modulation of the kv3.1b potassium channel isoform adjusts the fidelity of the firing pattern of auditory neurons. J. Neurosci. *23*, 1133–1141.

Marder, E., and Prinz, A.A. (2002). Modeling stability in neuron and network function: the role of activity in homeostasis. Bioessays *24*, 1145–1154.

Moreno, H., Vega-Saenz de Miera, E., Nadal, M.S., Amarillo, Y., and Rudy, B. (2001). Modulation of Kv3 potassium channels expressed in CHO cells by a nitric oxide-activated phosphatase. J. Physiol. *530*, 345–358.

Mottola, A., Antoniotti, S., Lovisolo, D., and Munaron, L. (2005). Regulation of noncapacitative calcium entry by arachidonic acid and nitric oxide in endothelial cells. FASEB J. *19*, 2075–2077.

Oertel, D. (1999). The role of timing in the brain stem auditory nuclei of vertebrates. Annu. Rev. Physiol. *61*, 497–519.

Palmer, R.M., Ferrige, A.G., and Moncada, S. (1987). Nitric oxide release accounts for the biological activity of endothelium-derived relaxing factor. Nature *327*, 524–526.

Rothman, J.S., and Manis, P.B. (2003). Kinetic analyses of three distinct potassium conductances in ventral cochlear nucleus neurons. J. Neurophysiol. *89*, 3083–3096.

Rudy, B., and McBain, C.J. (2001). Kv3 channels: voltage-gated K^+ channels designed for high-frequency repetitive firing. Trends Neurosci. *24*, 517–526.

Schneggenburger, R., and Forsythe, I.D. (2006). The calyx of Held. Cell Tissue Res. *326*, 311–337.

Smith, P.H., Joris, P.X., and Yin, T.C. (1998). Anatomy and physiology of principal cells of the medial nucleus of the trapezoid body (MNTB) of the cat. J. Neurophysiol. *79*, 3127–3142.

Son, H., Hawkins, R.D., Martin, K., Kiebler, M., Huang, P.L., Fishman, M.C., and Kandel, E.R. (1996). Long-term potentiation is reduced in mice that are doubly mutant in endothelial and neuronal nitric oxide synthase. Cell *87*, 1015–1023.

Song, P., Yang, Y., Barnes-Davies, M., Bhattacharjee, A., Hamann, M., Forsythe, I.D., Oliver, D.L., and Kaczmarek, L.K. (2005). Acoustic environment determines phosphorylation state of the Kv3.1 potassium channel in auditory neurons. Nat. Neurosci. *8*, 1335–1342.

Southam, E., and Garthwaite, J. (1993). The nitric oxide-cyclic GMP signalling pathway in rat brain. Neuropharmacology *32*, 1267–1277.

Spruston, N., Jonas, P., and Sakmann, B. (1995). Dendritic glutamate receptor channels in rat hippocampal CA3 and CA1 pyramidal neurons. J. Physiol. *482*, 325–352.

Tansey, E.P., Chow, A., Rudy, B., and McBain, C.J. (2002). Developmental expression of potassium-channel subunit Kv3.2 within subpopulations of mouse hippocampal inhibitory interneurons. Hippocampus *12*, 137–148.

von Gersdorff, H., and Borst, J.G. (2002). Short-term plasticity at the calyx of Held. Nat. Rev. Neurosci. *3*, 53–64.

Wang, L.Y., and Kaczmarek, L.K. (1998). High-frequency firing helps replenish the readily releasable pool of synaptic vesicles. Nature *394*, 384–388.

Wang, L.Y., Gan, L., Forsythe, I.D., and Kaczmarek, L.K. (1998). Contribution of the Kv3.1 potassium channel to high-frequency firing in mouse auditory neurones. J. Physiol. *509*, 183–194.

Wong, A.Y., Billups, B., Johnston, J., Evans, R.J., and Forsythe, I.D. (2006). Endogenous activation of adenosine A1 receptors, but not P2X receptors, during high-frequency synaptic transmission at the calyx of Held. J. Neurophysiol. *95*, 3336–3342.